

Dynamics of the spin-1/2 Ising two-leg ladder with four-spin plaquette interaction and transverse field

Wescley Luiz de Souza ^{1,2,*}, Érica de Mello Silva ^{2,†} and Paulo H. L. Martins ^{2,‡}

¹*Instituto de Educação, Ciência e Tecnologia de Mato Grosso—Campus Cuiabá
Rua Professora Zulmira Canavarros, 95, 78005-200 Cuiabá, MT, Brazil*

²*Universidade Federal de Mato Grosso, Instituto de Física, Av. Fernando Corrêa da Costa, 2367,
Bloco F, 78060-900 Cuiabá, MT, Brazil*

 (Received 10 December 2019; revised manuscript received 24 February 2020; accepted 9 March 2020; published 3 April 2020)

Multiple-spin coupling is a key tool for investigating magnetic quantum systems. In particular, models with four-spin interactions became of great interest since they have been applied to describe material properties such as superconductivity. In this framework, the dynamics of the spin-1/2 Ising two-leg ladder with four-spin plaquette interaction in a transverse field is investigated. By means of the recurrence relations method, the first four recurrants are determined exactly for the general model, while five exact recurrants are calculated for two particular models. In all cases, higher-order recurrants are computed through extrapolation to obtain time-dependent autocorrelation functions and spectral densities in the long-time regime and infinite-temperature limit. It is found that the relaxation functions decay slower than the expected behavior of the one-dimensional transverse Ising model. The spectral lines, characterized by a Lorentzian behavior in the central body and a Gaussian shape in the tails, display exchange narrowing as the coupling intensities increase.

DOI: [10.1103/PhysRevE.101.042104](https://doi.org/10.1103/PhysRevE.101.042104)

I. INTRODUCTION

Spin dynamics of quantum systems has been the object of countless research in the last decades to better understand phenomena associated with interactions between spins in magnetic systems [1], high-temperature superconductors [2], ferromagnetic nanowires [3], and spintronics [4]. More recently, a great interest in the dynamical properties of low-dimensional spin-1/2 models emerged due to experimental applications to ultracold atoms in optical lattices [5,6]. In this context, spin models of multiple interactions have been considered, since they provide a more realistic representation of physical systems, both experimentally and theoretically. Some of them are the Ising model with next-nearest-neighbor interactions [7] and with linear interaction of four spins [8–10], ladder models describing cuprates [11,12], and spin models with four-spin interactions [13–16], used to explain ferroelectrics [17,18].

Among the four-spin interactions, one finds the cyclic coupling [19–21], which has been applied to describe superconductivity in cuprates [22,23]. This interaction reproduces the observed dispersion relation in inelastic neutron scattering experiments for $\text{La}_6\text{Ca}_8\text{Cu}_{24}\text{O}_{41}$ [24]; besides, it is necessary for a quantitative understanding of the experimental results on spin gap, Raman peaks, and optical conductivity [25–27]. The plaquette interaction appears in a variation of the three-

dimensional Ising model, named the gonihedric model [28], which describes interacting closed surfaces without surface tension, covering areas from biochemistry to high-energy physics [29,30]. Furthermore, it arises in applications on thin films [31], quantum computation [32], and superconductor physics [33]. The static properties of most of these models have been well studied, but their dynamical properties have been barely explored, which in turn attracts a lot of interest. For instance, in a recent investigation on Ising ladder models with generalized plaquettes and transverse field, long relaxation times of edge spins due to strong zero modes were addressed [34]. Therefore, in this paper, the dynamics of the spin-1/2 Ising two-leg ladder model with four-spin plaquettes in a transverse magnetic field at the infinite-temperature limit is investigated by means of the recurrence relations method (RRM), developed by Lee [35,36].

The RRM is an orthogonalization approach that describes the time evolution of a dynamical variable in a geometric frame through the recurrants, which constitute a static property of the Hilbert space and are related to dynamical correlation functions [35–39]. The basis vectors of this orthogonal expansion are obtained recursively by applying a first recurrence relation, and the time-dependent expansion coefficients, which correspond to relaxation functions, obey a second recurrence relation [35,36]. The RRM has been successfully applied to study the dynamics of both quantum and classical systems [40–45], such as spin chains [46–60], Fermi liquids [61–66], harmonic oscillator chains [67–73], and plasmonic Dirac systems [74,75].

The aim of this paper is to obtain and characterize the time-dependent autocorrelation function and the spectral density

*wescley.souza@cba.ifmt.edu.br

†erica@fisica.ufmt.br

‡pmartins@fisica.ufmt.br

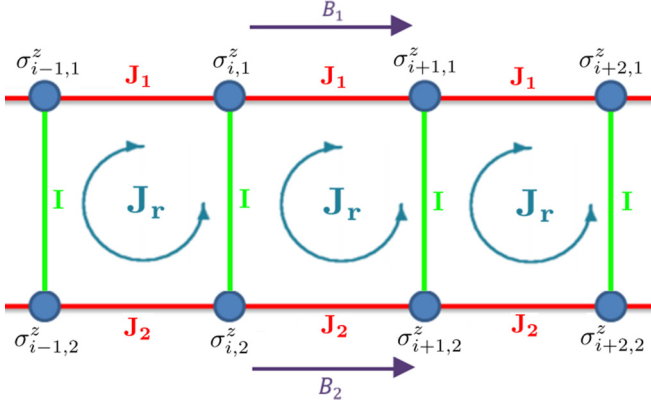


FIG. 1. Representation of the spin-1/2 Ising two-leg ladder with plaquette exchange and transverse field. J_1 (J_2) is the Ising interaction along chain 1 (2), I is the rung interaction, J_r is the four-spin plaquette exchange, and B_1 (B_2) is the transverse field in the chain 1 (2). The z direction is perpendicular to the plane.

for the Ising ladder with plaquette interaction and transverse field. The first four recurrants are exactly calculated for the general model, and one additional recurrant is obtained for two particular cases. The results are extended to longer times via an extrapolation, allowing us to analyze the relaxation and the spectral density functions for several combinations of the exchange interactions. The spectral lines are characterized by a Lorentzian behavior in the central body and a Gaussian shape in the wings, and it is verified that exchange narrowing takes place as the interactions increase.

The paper is organized as follows. In Sec. II, the model and the method are introduced. Section III presents the exact recurrants and their corresponding dynamical correlation functions. In Sec. IV, extrapolated results are discussed. Concluding remarks close the last section.

II. MODEL AND METHOD

The following Hamiltonian is considered:

$$\begin{aligned} \mathcal{H} = & -J_1 \sum_{i=1}^N \sigma_{i,1}^z \sigma_{i+1,1}^z - J_2 \sum_{i=1}^N \sigma_{i,2}^z \sigma_{i+1,2}^z \\ & - I \sum_{i=1}^N \sigma_{i,1}^z \sigma_{i,2}^z - J_r \sum_{i=1}^N \sigma_{i,1}^z \sigma_{i+1,1}^z \sigma_{i+1,2}^z \sigma_{i,2}^z \\ & - B_1 \sum_{i=1}^N \sigma_{i,1}^x - B_2 \sum_{i=1}^N \sigma_{i,2}^x, \end{aligned} \quad (1)$$

where N is the number of spins in each leg, $\sigma_{i,j}^\alpha$ ($\alpha = x, z; j = 1, 2$) are spin operators defined by Pauli matrices on site i of chain j , J_1 (J_2) is the nearest-neighbor exchange interactions along the chain 1 (2), I is the interchain (rung) Ising coupling, J_r is the four-spin plaquette interaction, and B_1 (B_2) is the external transverse field acting on chain 1 (2). A schematic representation is illustrated in Fig. 1.

The dynamical variable of interest is the z component of a spin operator in chain 1, $\sigma_{k,1}^z(t)$, whose time evolution is

governed by the Heisenberg equation,

$$\frac{d\sigma_{k,1}^z(t)}{dt} = i[\mathcal{H}, \sigma_{k,1}^z], \quad (2)$$

with $\hbar = 1$. In the RRM, the time evolution of a dynamical variable is studied in a geometric frame. For times $t \geq 0$, the tagged spin operator $\sigma_{k,1}^z(t)$ is written as an orthogonal expansion,

$$\sigma_{k,1}^z(t) = \sum_{v=0}^{d-1} f_v a_v(t), \quad (3)$$

where $\{a_v\}$ is a set of time-dependent functions representing the projections of $\sigma_{k,1}^z(t)$ onto the time-independent orthogonal basis vectors $\{f_v\}$. The Hilbert space \mathcal{S} has dimensionality d and is realized by an inner product called the Kubo product [35,37–39], defined by

$$(X, Y) = \beta^{-1} \int_0^\beta d\lambda \langle X(\lambda) Y^\dagger \rangle - \langle X \rangle \langle Y^\dagger \rangle, \quad (4)$$

in which X and $Y \in \mathcal{S}$ are Hermitian operators, $\beta = 1/k_B T$, k_B is the Boltzmann constant, T is the temperature, $X(\lambda) = \exp(\lambda \mathcal{H}) X \exp(-\lambda \mathcal{H})$, and $\langle XY^\dagger \rangle = \text{Tr}[XY^\dagger \exp(-\beta \mathcal{H})] / \text{Tr}[\exp(-\beta \mathcal{H})]$ is the canonical ensemble average. At the infinite-temperature limit, the Kubo product (4) reduces to [76]

$$(X, Y) = \frac{1}{Z} \text{Tr}[XY^\dagger], \quad (5)$$

where Z is the partition function.

The realization of \mathcal{S} by the Kubo product leads to a recurrence relation for the basis vectors,

$$f_{v+1} = i[\mathcal{H}, f_v] + \Delta_v f_{v-1}, \quad 0 \leq v \leq d-2, \quad (6)$$

where Δ_v , called v recurrant, is given by

$$\Delta_v = \frac{(f_v, f_v)}{(f_{v-1}, f_{v-1})}. \quad (7)$$

The relation (6) shall be referred to as RR I. By definition, $\Delta_0 \equiv 1$ and $f_{-1} \equiv 0$. Once $f_0 = \sigma_{k,1}^z(0)$ is chosen, the remaining basis vectors are obtained recursively by RR I (6) and the recurrants (7). The coefficients $a_v(t)$, which are relaxation functions, are determined from the second recurrence relation (RR II),

$$\Delta_{v+1} a_{v+1}(t) = -\dot{a}_v(t) + a_{v-1}(t), \quad 0 \leq v \leq d-2, \quad (8)$$

where $\dot{a}_v(t) = da_v(t)/dt$ and $a_{-1} \equiv 0$.

The choice of $\sigma_{k,1}^z$ as the dynamical variable implies that the coefficient $a_0(t)$ corresponds to the time-dependent auto-correlation function $C_z(t)$,

$$a_0(t) = (\sigma_{k,1}^z, \sigma_{k,1}^z(t)) = \frac{1}{Z} \text{Tr}[\sigma_{k,1}^z \sigma_{k,1}^z(t)] \equiv C_z(t). \quad (9)$$

The function $C_z(t)$ can be evaluated by

$$C_z(t) = \sum_{v=0}^{\infty} \frac{(-1)^v}{(2v)!} \mu_{2v} t^{2v}, \quad (10)$$

where the moments μ_{2v} are [76]

$$\mu_2 = \Delta_1, \quad \mu_4 = \Delta_1(\Delta_1 + \Delta_2), \quad (11)$$

$$\mu_6 = \Delta_1[(\Delta_1 + \Delta_2)^2 + \Delta_2 \Delta_3], \dots, \quad (12)$$

with lengthier expressions for higher-order moments. By taking the Laplace transform of RR II (8), one reaches

$$1 = z\tilde{a}_0(z) + \Delta_1\tilde{a}_1(z), \quad (13a)$$

$$\tilde{a}_{\nu-1}(z) = z\tilde{a}_\nu(z) + \Delta_{\nu+1}\tilde{a}_{\nu+1}(z), \quad (13b)$$

where $\tilde{a}_\nu(z)$ is the Laplace transform of $a_\nu(t)$. By using Eqs. (13a) and (13b), the continued fraction representation for $\tilde{a}_0(z)$ is written as

$$\tilde{a}_0(z) = \frac{1}{z + \frac{\Delta_1}{z + \frac{\Delta_2}{z + \frac{\Delta_3}{z + \dots}}}}, \quad (14)$$

which implies the existence of a d -dimensional space defined by the set of recurrants Δ_ν . Therefore, once one knows the basal function $\tilde{a}_0(z)$, the remaining relaxation functions can be readily calculated through RR II (8).

The spectral density $S_z(\omega)$ is defined as the time Fourier transform of the relaxation function $C_z(t)$ [76],

$$S_z(\omega) = \int_{-\infty}^{+\infty} C_z(t) e^{-i\omega t} dt, \quad (15)$$

and it can also be directly obtained from $\tilde{a}_0(z)$ [77]:

$$S_z(\omega) = \lim_{\epsilon \rightarrow 0^+} \text{Re}[2\tilde{a}_0(\epsilon - i\omega)]. \quad (16)$$

In the RRM approach, the recurrants Δ_ν are the key quantities to be determined. Their analytical calculation, however, usually involves an intractable amount of terms and, in general, only the first ones are known. For most cases, one must resort to an extrapolation, such as the Gaussian terminator [76] or numerical approaches [50,51] in order to get higher-order Δ s.

III. EXACT RESULTS FOR THE BASIS VECTORS

The basis vector f_0 corresponds to the dynamical variable $\sigma_{k,1}^z(0)$, and its norm is $(f_0, f_0) = 1$. To determine f_1 , RR I is applied with $\nu = 0$:

$$f_1 = i[\mathcal{H}, f_0] = i[\mathcal{H}, \sigma_{k,1}^z]. \quad (17)$$

For the general model (1), it is given by

$$f_1 = -2B_1\sigma_{k,1}^y, \quad (18)$$

and the recurrant Δ_1 is determined:

$$\Delta_1 = 4B_1^2. \quad (19)$$

The next basis vector is f_2 . Applying RR I with $\nu = 1$, one has

$$f_2 = i[\mathcal{H}, f_1] + \Delta_1 f_0, \quad (20)$$

and the expression for f_2 reads as

$$\begin{aligned} f_2 = & 4J_1 B_1 \sigma_{k-1,1}^z \sigma_{k,1}^x + 4J_1 B_1 \sigma_{k,1}^x \sigma_{k+1,1}^z \\ & + 4I B_1 \sigma_{k,1}^x \sigma_{k,2}^z + 4J_r B_1 \sigma_{k-1,1}^z \sigma_{k,1}^x \sigma_{k-1,2}^z \sigma_{k,2}^x \\ & + 4J_r B_1 \sigma_{k,1}^x \sigma_{k+1,1}^z \sigma_{k,2}^z \sigma_{k+1,2}^x. \end{aligned} \quad (21)$$

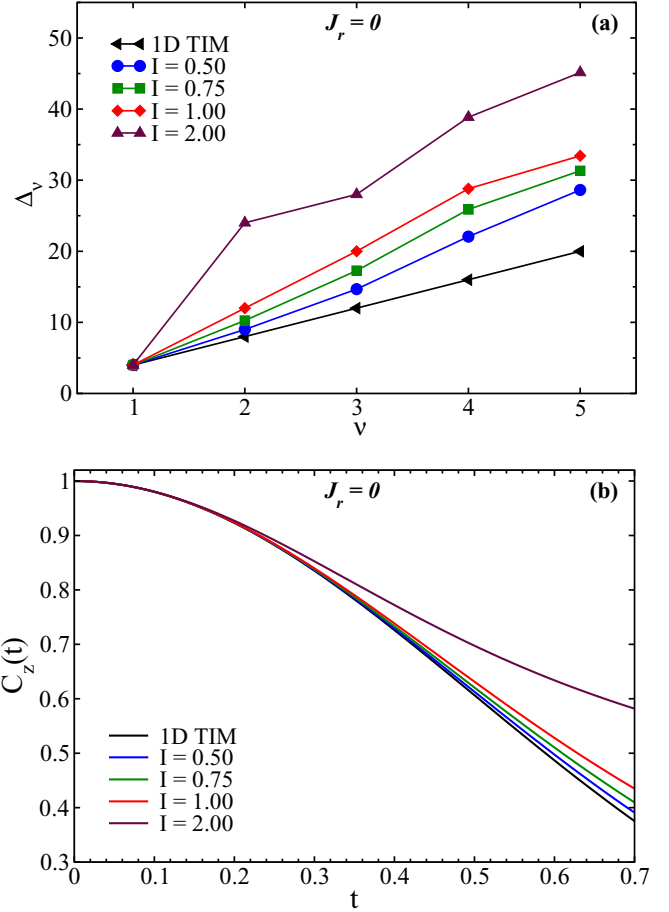


FIG. 2. (a) Exact recurrants of the standard two-leg ladder Ising model ($J_r = 0$), for $J_1 = J_2 = B_1 = B_2 = 1.0$, and different values of the rung coupling I , together with the 1D TIM from Ref. [46]. (The lines connecting the symbols are just an aid to the eye.) (b) Time-dependent spin autocorrelation functions $C_z(t)$ evaluated from the exact recurrants. The expected Gaussian decay (1D TIM) is also shown for the sake of comparison.

The second recurrant is then

$$\Delta_2 = 8J_1^2 + 4I^2 + 8J_r^2. \quad (22)$$

By following this recipe, the next basis vectors, f_3 and f_4 , and recurrants, Δ_3 and Δ_4 , are calculated; their expressions, however, are too lengthy to be reproduced here. Therefore, for the general model (1), the first four basis vectors of the realized Hilbert space of $\sigma_{k,1}^z(t)$ are exactly computed. Hereafter, two particular cases are analyzed: (i) without the plaquette interaction ($J_r = 0$) and (ii) with it, but without the two-spin interchain coupling ($I = 0$). For such reduced models, it is still manageable to evaluate one additional vector, f_5 , and recurrant, Δ_5 . The coupling parameters are set as $J_1 = J_2 = 1.0$ and the fields as $B_1 = B_2 = 1.0$ (in units of J). The interchain coupling I and the plaquette interaction J_r are also measured in units of J .

The particular case ($I \neq 0, J_r = 0$) corresponds to the standard ladder with two-spin interchain interaction. To have a picture of the recurrants, the first five Δ_ν ($\nu = 1, \dots, 5$) are shown in Fig. 2(a) for $J_r = 0$ and several values of the rung

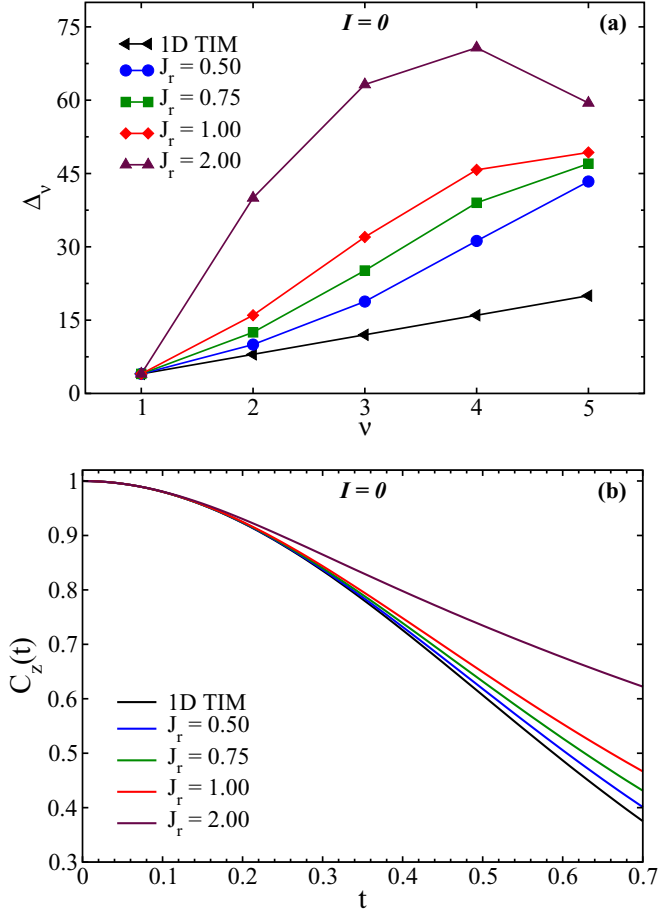


FIG. 3. (a) Exact recurrants of the Ising ladder with $I = 0$, $J_1 = J_2 = B_1 = B_2 = 1.0$, and some values of the plaquette interaction J_r . (The lines connecting the symbols are just an aid to the eye.) (b) Time-dependent spin autocorrelation functions $C_z(t)$ obtained from the first five recurrants.

interaction I . For the sake of comparison, the recurrants of the one-dimensional transverse Ising model (1D TIM)—which corresponds to $(I = 0, J_r = 0)$ [46], are also shown. It is noticeable that increasing I makes the recurrants grow at a higher rate, on average.

Figure 2(b) shows the autocorrelation functions $C_z(t)$, given by Eq. (10), with the moments evaluated from the first five recurrants. For $J_1 = B_1 = 1.0$, the expected behavior of the 1D TIM is $C_z(t) \sim \exp(-2t^2)$ [78,79]; it also appears in Fig. 2(b) on account of comparison. The exact recurrants provided reliable results up to time $t \approx 0.7$ (measured in units of the inverse of the exchange interaction, J^{-1}).

Analogously, the case where the legs are coupled through plaquette interaction only ($I = 0, J_r \neq 0$) is analyzed. In Fig. 3(a), the first five exact Δ_ν for $I = 0$ and some values of J_r are shown. Similarly to the standard Ising two-leg ladder model, there is an irregular character in the sequences of the recurrants as J_r increases [46]. The autocorrelation functions are presented in Fig. 3(b) for some values of J_r and also for the 1D TIM. In the latter case, $C_z(t)$ decays faster. The results are reliable up to time $t \approx 0.7$.

Regarding the general model (1), the behavior of the first recurrants resembles the ones of the particular cases exploited.

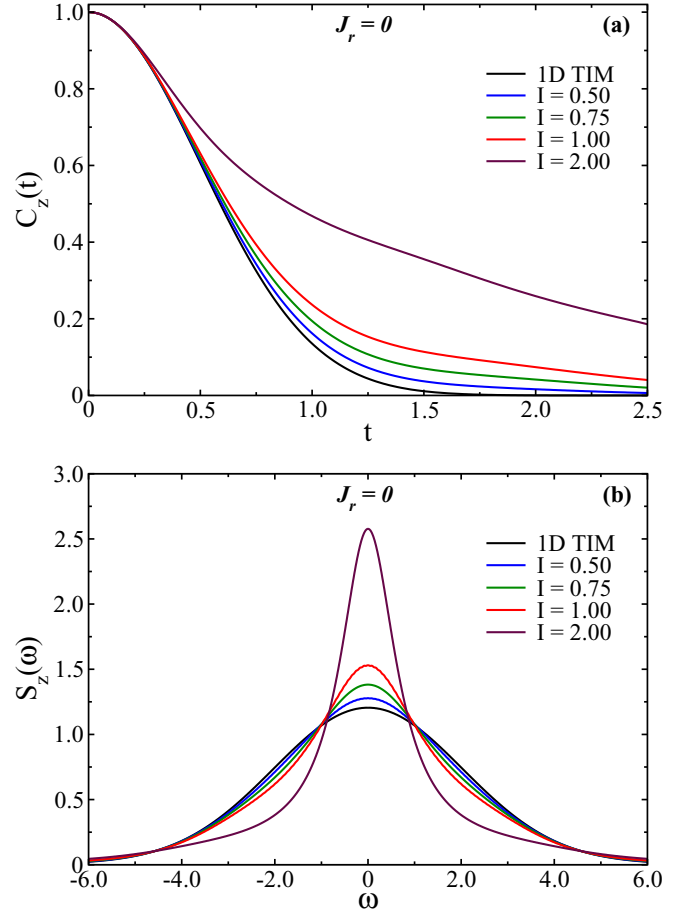


FIG. 4. (a) Time-dependent correlation functions for $J_r = 0$, $J_1 = J_2 = B_1 = B_2 = 1.0$, and some values of I , using 100 recurrants Δ_ν . The exact Gaussian decay of the 1D TIM is also shown on account of comparison (black line). (b) Spectral densities obtained from Eq. (16). They also correspond to the Fourier transforms of the correlation functions shown in (a).

For smaller values of I and J_r , the recurrants Δ_ν increase almost linearly with ν and the ensuing time-dependent correlation function is valid for relatively short times. From now on, to get higher-ordered recurrants to extend the time domain, some sort of numerical approximation is considered, since hand calculation is quite prohibitive for the Hamiltonian (1) and its particular cases.

IV. EXTRAPOLATED RESULTS

A. Spin-1/2 Ising ladder model ($I \neq 0, J_r = 0$)

A linear growth of the recurrants has already been observed on variations of the Ising model [7,54,56–58]. According to Figs. 2 and 3, for $I \lesssim 2.0$ and $J_r \lesssim 1.0$, the behavior of the first five recurrants does not deviate too much from a linear fit. Thus, the proposed extrapolation is $\Delta_\nu = a\nu + b$, $\nu \geq 6$, where the parameters a and b are determined from a linear regression of the exact recurrants. The 1D TIM corresponds to $b = 0$ [46].

Figure 4(a) shows the time-dependent correlation function for $J_1 = J_2 = B_1 = B_2 = 1.0$ and several values of I using

100 recurrants. It is found that the relaxation function $C_z(t)$ has a slower decay compared to that of the 1D TIM, for which the decay is an exact Gaussian [7,78,79]. For higher values of I , the decay slowed down even more, leading the tagged spin $\sigma_{k,1}^z$ to delay its relaxation process toward an equilibrium state. It is worth mentioning that the short-time regime is well captured by the first recurrants, since for $t \leq 0.7$ the curves are identical to the ones in Fig. 2(b).

A recent work [59] shows the spectral density being evaluated from the Fourier transform of the correlation function, as in Eq. (15), which allows us to get $S_z(\omega)$ for some discrete values of ω only. A noteworthy feature of the present work is the evaluation of $S_z(\omega)$ from $\tilde{a}_0(z)$, which is directly determined from the set of Δ_ν . This approach provides a smooth spectral density for any frequency range.

The spectral density $S_z(\omega)$, evaluated from Eq. (16), is depicted in Fig. 4(b) for different values of the interchain coupling I . For a given frequency ω and parameter ϵ , one sets $z = \epsilon - i\omega$ and $\tilde{a}_0(z)$ is computed from Eq. (14). Variation of ϵ allows us to obtain the limiting behavior $\epsilon \rightarrow 0^+$ and thus the spectral density for that frequency ω . Repeating this process for several values of ω gives the continuouslike function $S_z(\omega)$. In this investigation, a range of values of ϵ , both greater and smaller than 0.1, is tested to analyze the limit $\epsilon \rightarrow 0^+$, which ensures that $\epsilon = 0.1$ is suitable for the current analysis.

The Gaussian $S_z(\omega)$, corresponding to the 1D TIM, is also plotted in Fig. 4(b). The present approach is corroborated at this limiting case. Furthermore, one can observe in the spectral density that, as the intensity of I increases, there is an enhancement of the central peak, which becomes higher and narrower, highlighting the dominant central mode behavior.

The specific shapes of $C_z(t)$ and $S_z(\omega)$ are analyzed in Fig. 5. As an example, for $I = 1.0$ and $J_r = 0.0$, in the short-time regime ($t \lesssim 0.5$), the autocorrelation function is well adjusted by a Gaussian line, as displayed in Fig. 5(a). For longer times ($t \gtrsim 1.3$), an exponential fit is observed. A transition between both forms occurs in the region $0.5 \lesssim t \lesssim 1.3$. As the spectrum $S_z(\omega)$ and the autocorrelation function $C_z(t)$ are mutually Fourier transforms, the spectral density central part assumes a Lorentzian form, while the high-frequency region presents a Gaussian behavior. For the sake of clarity, Fig. 5 comprises other values of I and J_r , which will be discussed ahead.

B. Spin-1/2 Ising ladder with plaquette interaction ($I = 0, J_r \neq 0$)

The routine is analogous to the one described above. Considering 100 recurrants, the time-dependent correlation functions for $J_1 = J_2 = B_1 = B_2 = 1.0$ and several values of J_r (and the exact correlation function of the 1D TIM) are shown in Fig. 6(a). The relaxation function $C_z(t)$ diminishes slower than the one for the 1D TIM, and the decay becomes even slower for higher values of J_r . It should be attributed to the fact that the plaquette interaction involves four spins (two in each leg), so the dynamical variable $\sigma_{k,1}^z$ takes a longer time for relaxing towards an equilibrium state. As time runs, $C_z(t)$ changes from Gaussian to exponential, as shown in Fig. 5(a).

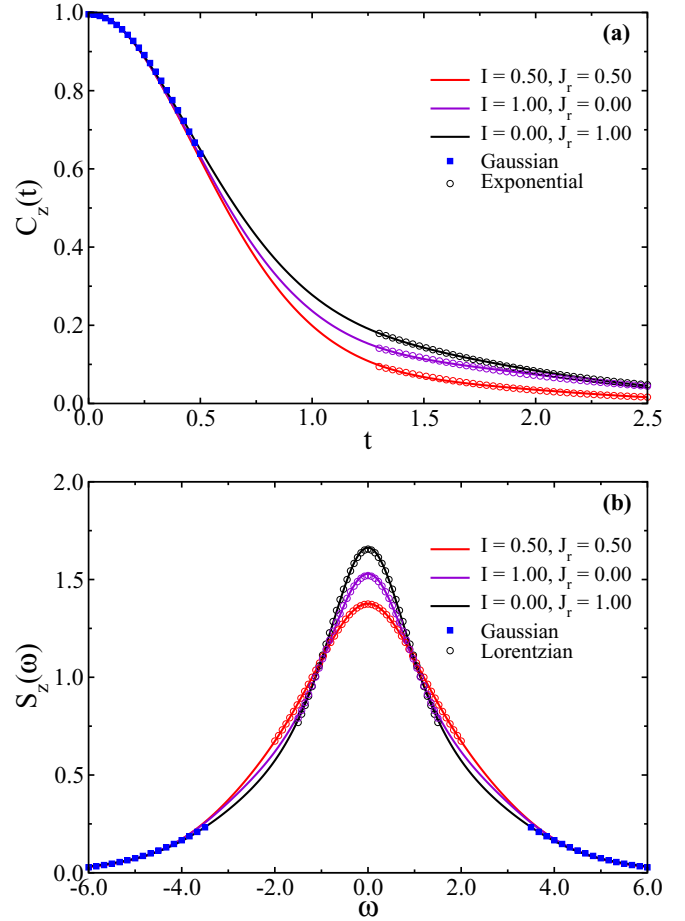


FIG. 5. (a) Best fits for the autocorrelation functions. At short times, the Gaussian decay is observed (blue squares). For clarity, only the fit corresponding to $I = 0.0$ and $J_r = 1.0$ is shown in this region. For longer times, the best fits are exponential (open circles). A transition between both forms occurs in the region $0.5 \lesssim t \lesssim 1.3$. (b) Spectral density line shape. The results are very well adjusted by a combination of a Lorentzian peak (for $|\omega| \lesssim 2.0$) and Gaussian wings ($|\omega| \gtrsim 3.3$). A transition between both regimes is observed in the region $2.0 \lesssim |\omega| \lesssim 3.3$. Similar behavior is detected for other values of I and J_r .

Figure 6(b) presents the spectral density for several values of the plaquette interaction J_r and the known Gaussian curve for the 1D TIM. Similarly to the previous case, the increase of J_r brings forth the Lorentzian character of the central peak around $\omega = 0$, which remains dominant in the dynamics, as displayed in Fig. 5(b).

C. Spin-1/2 Ising ladder with plaquette and rung interactions ($I \neq 0, J_r \neq 0$)

The general case ($I \neq 0, J_r \neq 0$) is now considered using 100 recurrants. Figure 7(a) brings the time-dependent correlation functions for $J_1 = J_2 = B_1 = B_2 = 1.0$ and different values of I and J_r . With both two- and four-spin interactions combined, the relaxation function decay is slower than in any of those particular cases already investigated. Therefore, the tagged spin $\sigma_{k,1}^z$ continues to lag its relaxation process toward an equilibrium state if compared to the 1D TIM. Nevertheless,

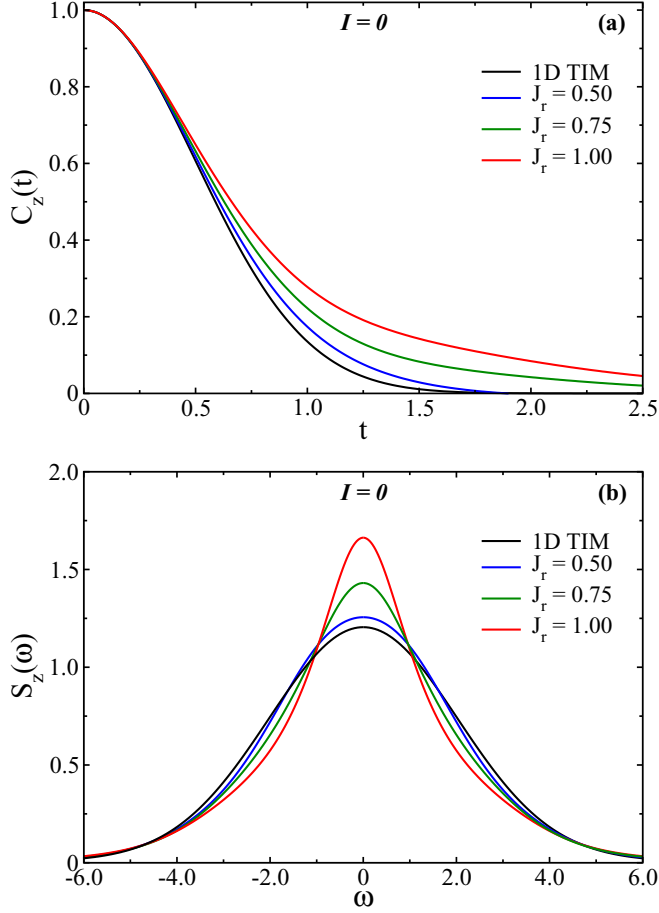


FIG. 6. (a) Time-dependent correlation functions for $I = 0$, $J_1 = J_2 = B_1 = B_2 = 1.0$, and different values of J_r , using 100 recurrants Δ_ν . (b) Corresponding spectral densities.

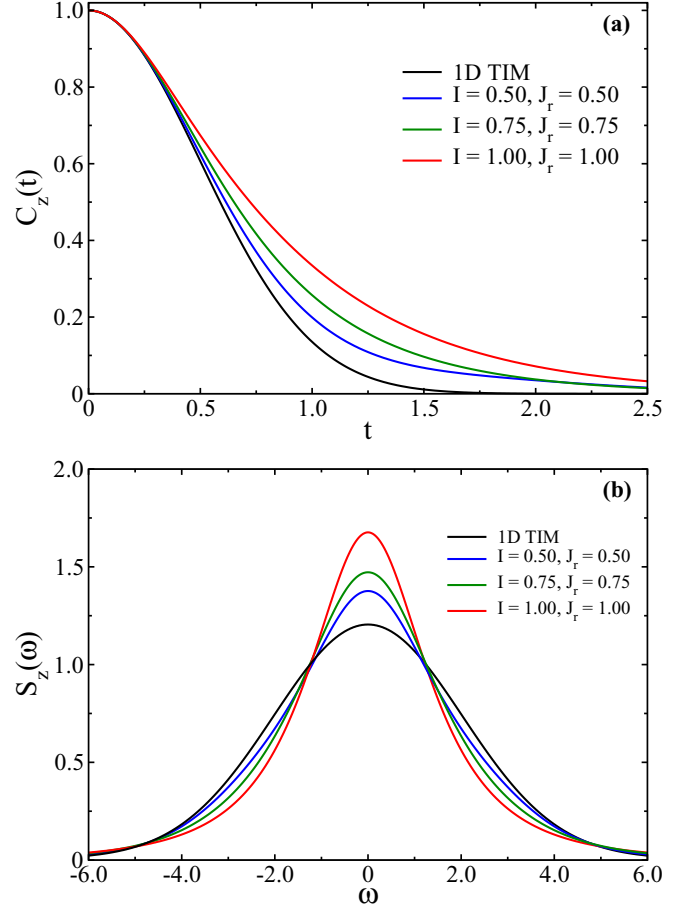


FIG. 7. (a) Correlation functions $C_z(t)$ for $J_1 = J_2 = B_1 = B_2 = 1.0$ and some values of I and J_r , using 100 recurrants Δ_ν . (b) Corresponding spectral densities.

regarding the cases ($I = 0.5$, $J_r = 0.5$) and ($I = 0.75$, $J_r = 0.75$), one observes the correlation functions crossing each other at $t \approx 2.1$. From that time on, $C_z(t)$ decays faster for ($I = 0.75$, $J_r = 0.75$).

Figure 7(b) shows the corresponding spectral densities for the values of I and J_r depicted in Fig. 7(a). One notices that the increase of the coupling intensity also raises the central peak around $\omega = 0$. This rise is more pronounced than in the particular cases previously discussed, and this phenomenon can be better understood by inspecting Fig. 5.

For the ($I = 0.5$, $J_r = 0.5$) case, the relaxation function is depicted in Fig. 5(a) and the spectral density in Fig. 5(b). By comparing the spectral lines, the exchange narrowing is observed as the interchain couplings change. The Kubo-Tomita (KT) line-shape theory explains this phenomenon satisfactorily for three-dimensional systems [80]. The KT approach, however, presents some limitations when applied to low-dimensional systems due to the presence of spin diffusion at the long-time regime [81]. In the present model, although in low dimension, the interchain couplings seem to dominate the regulation of the linewidth spectra, leading the spin correlations to decay in a similar behavior as of three-dimensional systems [82]. Furthermore, this investigation is carried out in

the infinite-temperature limit, at which the validity of the KT theory is well established [81,82].

Figure 8(a) compares the autocorrelation functions for all cases described in this section, for several values of I and J_r . By inspecting the effects of the two- and four-spin interactions separately, say for instance ($I = 0.5$, $J_r = 0$), blue line, and ($I = 0$, $J_r = 0.5$), green line, one can see that the plaquette interaction leads to a slower decay of the correlation function for times $t \lesssim 1.3$. For longer t , however, the model with nonzero plaquette exchange decays faster. A similar change in the behavior of the correlation function can be noted if one compares ($I = 1.0$, $J_r = 0$), in purple, to ($I = 1.0$, $J_r = 1.0$), in pink, at $t \approx 1.9$. It seems that the combination of interactions changes the behavior of the correlation function at longer times.

Figure 8(b) shows the spectral densities corresponding to the correlation functions plotted in Fig. 8(a). For all $S_z(\omega)$ curves, the dynamics is dominated by the central mode. By confronting the effects of the exchange interactions, for higher intensities one observes that the sharpening of the curve is more pronounced for ($I = 1.0$, $J_r = 1.0$), in pink, followed by ($I = 0$, $J_r = 1.0$), in black, and then by ($I = 1.0$, $J_r = 0$), in purple. Nevertheless, for lower intensities, the sequence of enhancements is ($I = 0.5$, $J_r = 0.5$), red line, ($I = 0.5$,

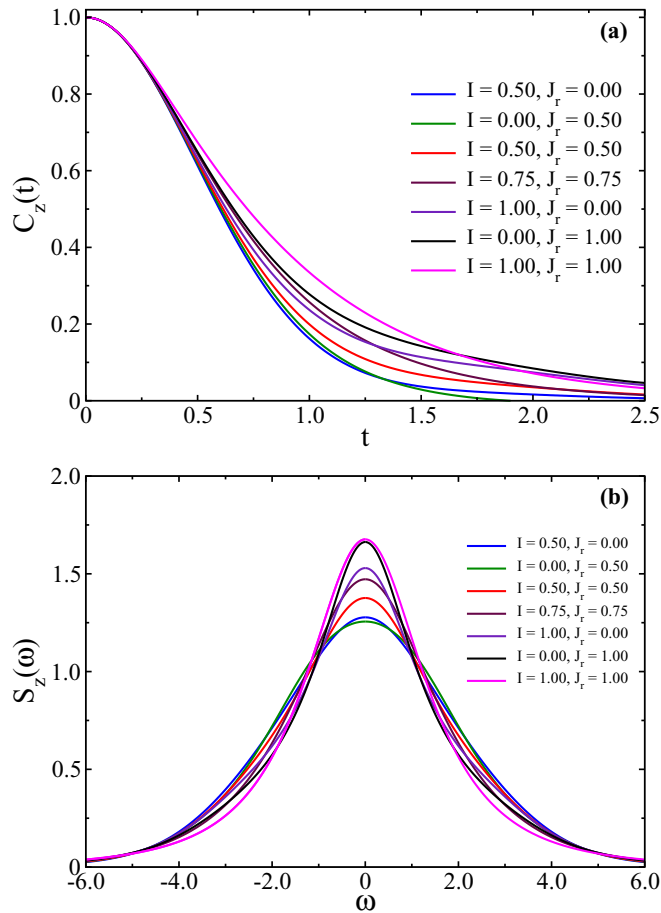


FIG. 8. (a) Time-dependent correlation functions for particular cases and the general model. We used the first four (general model) and five (cases $J_r = 0$ and $I = 0$) exact recurrants besides the extrapolated ones up to $\nu = 100$. (b) Corresponding spectral densities.

$J_r = 0$) in blue, and ($I = 0, J_r = 0.5$) in green. Therefore, the combination of two- and four-spin interactions always fosters the central mode behavior, but the intensity of the interactions plays a pivotal role when only the plaquette or the interchain coupling is present.

V. CONCLUDING REMARKS

In this paper, the dynamics of the spin-1/2 Ising two-leg ladder with plaquette interaction and transverse field at the

infinite-temperature limit is investigated. By means of the RRM, the first four recurrants are computed for the general model (1); for the standard Ising two-leg ladder ($I \neq 0, J_r = 0$) and the ladder with plaquette interaction ($I = 0, J_r \neq 0$), five exact recurrants are calculated. These exact recurrants provide reliable results in the short-time domain. Additionally, higher-order recurrants, obtained from an extrapolation scheme, allow the computation of long-time relaxation functions and their associated spectral densities. The time evolution of $\sigma_{k,1}^z(t)$ is analyzed for several combinations of the two-spin coupling and the plaquette interaction intensities. In all cases, the dynamical variable takes a longer time for relaxing toward an equilibrium state in comparison with the 1D TIM. In the same footing, an increase in the intensity of the interactions I and J_r leads to the exchange narrowing phenomenon, according to which the central body of the spectral density $S_z(\omega)$ becomes more and more Lorentzian, indicating the central mode dominance in the dynamics. Meanwhile, the wings of $S_z(\omega)$ maintain their Gaussian shape. There are, however, intriguing peculiarities in the dynamics of some cases, depending upon the intensity level of the interactions. By confronting the effects of the interchain interactions, one would expect the sharpening of $S_z(\omega)$ to be more pronounced for a given value of J_r than for the same value of I , since the plaquette interaction involves four spins. In fact, it is verified that it is true for higher values of J_r . From Fig. 8(b), the observed exchange narrowing phenomenon is higher for ($I = 0, J_r = 1.0$), black curve, than for ($I = 1.0, J_r = 0$), purple line. Conversely, for the intensity 0.5, the two-spin interaction I is more effective than the four-spin coupling J_r , as remarked by a comparison between the blue and green curves [Fig. 8(b)]. Exchange narrowing of the combination of I and J_r , both nonzero, is more pronounced in all analyzed cases. These behaviors point out the richness of the dynamics of the spin-1/2 Ising two-leg ladder model with plaquettes in a transverse magnetic field at the infinite-temperature limit. We believe that such results can be useful in the characterization of electron paramagnetic resonance spectroscopy of low-dimensional systems. In a forthcoming work, the effects of randomness in the external transverse field shall be addressed.

ACKNOWLEDGMENTS

The authors gratefully thank M. E. S. Nunes for drawing their attention to this model. Fruitful discussions with the members of GRUDI Research Group is appreciated. Brazilian agency CAPES is acknowledged for partial financial support.

[1] W. D. Ratcliff and J. W. Lynn, *Multiferroics*, in *Neutron Scattering—Magnetic and Quantum Phenomena*, Experimental Methods in the Physical Sciences, Vol. 48, edited by F. Fernandez-Alonso and D. L. Price (Elsevier, Cambridge, 2015), Chap. 5, pp. 291–338.
 [2] P. A. Lee, N. Nagaosa, and X.-G. Wen, *Rev. Mod. Phys.* **78**, 17 (2006).
 [3] J. Cho, Y. Fujii, K. Konishi, J. Yoon, N. Kim, J. Jung, S. Miwa, M. Jung, Y. Suzuki, and C. You, *J. Magn. Magn. Mater.* **409**, 99 (2016).

[4] I. Žutić, J. Fabian, and S. D. Sarma, *Rev. Mod. Phys.* **76**, 323 (2004).
 [5] C. Karrasch, D. M. Kennes, and F. Heidrich-Meisner, *Phys. Rev. B* **91**, 115130 (2015).
 [6] Z. Liu, S. Jiang, X. Kong, and Y. Xu, *Physica A* **473**, 536 (2017).
 [7] P. R. C. Guimarães, J. A. Plascak, O. F. de Alcantara Bonfim, and J. Florencio, *Phys. Rev. E* **92**, 042115 (2015).
 [8] B. Boechat, J. Florencio, A. Saguia, and O. F. de Alcantara Bonfim, *Phys. Rev. E* **89**, 032143 (2014).

- [9] O. F. de Alcantara Bonfim, A. Saguia, B. Boechat, and J. Florencio, *Phys. Rev. E* **90**, 032101 (2014).
- [10] O. F. de Alcantara Bonfim and J. Florencio, *Phys. Rev. B* **74**, 134413 (2006).
- [11] G. T. Hohensee, R. B. Wilson, J. P. Feser, and D. G. Cahill, *Phys. Rev. B* **89**, 024422 (2014).
- [12] M. S. Naseri and S. Mahdaviifar, *Physica A* **474**, 107 (2017).
- [13] M. Ghliyem, N. Benayad, and M. Azhari, *Physica A* **402**, 14 (2014).
- [14] N. Benayad and M. Ghliyem, *J. Magn. Magn. Mater.* **343**, 99 (2013).
- [15] A. Jabar, R. Masrour, K. Jetto, L. Bahmad, A. Benyoussef, and M. Hamedoun, *Superlattices Microstruct.* **100**, 818 (2016).
- [16] A. Jabar, N. Tahiri, K. Jetto, and L. Bahmad, *Superlattices Microstruct.* **104**, 46 (2017).
- [17] W. Chunle, Q. Zikai, and Z. Jinghbo, *Ferroelectrics* **77**, 21 (1988).
- [18] B. H. Teng and H. K. Sy, *Europhys. Lett.* **73**, 601 (2006).
- [19] M. Müller, T. Vekua, and H.-J. Mikeska, *Phys. Rev. B* **66**, 134423 (2002).
- [20] A. Läuchli, G. Schmid, and M. Troyer, *Phys. Rev. B* **67**, 100409(R) (2003).
- [21] S. Nishimoto and M. Arikawa, *Phys. Rev. B* **79**, 113106 (2009).
- [22] C. B. Larsen, A. T. Romer, S. Janas, F. Treue, B. Monsted, N. E. Shaik, H. M. Ronnow, and K. Lefmann, *Phys. Rev. B* **99**, 054432 (2019).
- [23] R. Coldea, S. M. Hayden, G. Aeppli, T. G. Perring, C. D. Frost, T. E. Mason, S.-W. Cheong, and Z. Fisk, *Phys. Rev. Lett.* **86**, 5377 (2001).
- [24] M. Matsuda, K. Katsumata, R. S. Eccleston, S. Brehmer, and H.-J. Mikeska, *Phys. Rev. B* **62**, 8903 (2000).
- [25] S. Brehmer, H.-J. Mikeska, M. Müller, N. Nagaosa, and S. Uchida, *Phys. Rev. B* **60**, 329 (1999).
- [26] K. Schmidt, C. Knetter, and G. Uhrig, *Europhys. Lett.* **56**, 877 (2001).
- [27] T. S. Nunner, P. Brune, T. Kopp, M. Windt, and M. Grüninger, *Acta Phys. Pol. B* **34**, 1545 (2003).
- [28] G. K. Savvidy and F. J. Wegner, *Nucl. Phys. B* **413**, 605 (1994).
- [29] Y. Nishiyama, *Phys. Rev. E* **70**, 026120 (2004).
- [30] D. A. Johnston, M. Mueller, and W. Janke, *Eur. Phys. J.: Spec. Top.* **226**, 749 (2017).
- [31] S. Bouhou, A. Zaim, A. Ainane, M. Kerouad, and R. Ahuja, *J. Magn. Magn. Mater.* **339**, 127 (2013).
- [32] Y. Yang, Y. P. Xu, and S. Q. Zhu, *Eur. Phys. J. D* **61**, 751 (2011).
- [33] A. A. Katanin and A. P. Kampf, *Phys. Rev. B* **66**, 100403(R) (2002).
- [34] L. M. Vasiloiu, F. Carollo, M. Marcuzzi, and J. P. Garrahan, *Phys. Rev. B* **100**, 024309 (2019).
- [35] M. Lee, *Phys. Rev. Lett.* **49**, 1072 (1982).
- [36] M. Lee, *Phys. Rev. Lett.* **51**, 1227 (1983).
- [37] M. H. Lee, J. Hong, and J. Florencio, *Phys. Scr.* **T19B**, 498 (1987).
- [38] M. Lee, *Phys. Rev. E* **61**, 3571 (2000).
- [39] U. Balucani, M. H. Lee, and V. Tognetti, *Phys. Rep.* **373**, 409 (2003).
- [40] S. Sen, *Physica A* **315**, 150 (2002).
- [41] A. V. Mokshin, *Theor. Math. Phys.* **183**, 449 (2015).
- [42] I. Sawada, *Phys. A* **315**, 14 (2002).
- [43] S. Sen, *Physica A* **360**, 304 (2006).
- [44] A. V. Mokshin, *Discontinuity, Nonlinearity, and Complexity* **2**, 43 (2013).
- [45] A. S. T. Pires, *Helv. Phys. Acta* **61**, 988 (1988).
- [46] J. Florencio and M. H. Lee, *Phys. Rev. B* **35**, 1835 (1987).
- [47] J. Florencio and M. H. Lee, *Nucl. Phys. B* **5**, 250 (1988).
- [48] J. Florencio, S. Sen, and M. H. Lee, *Braz. J. Phys.* **30**, 725 (2000).
- [49] M. E. S. Nunes, J. A. Plascak, and J. Florencio, *Physica A* **332**, 1 (2004).
- [50] Maria Eugenia Silva Nunes and J. Florencio, *Phys. Rev. B* **68**, 014406 (2003).
- [51] S. Sen, Z.-X. Cai, and S. D. Mahanti, *Phys. Rev. E* **47**, 273 (1993).
- [52] Z.-Q. Liu, X.-M. Kong, and X.-S. Chen, *Phys. Rev. B* **73**, 224412 (2006).
- [53] S.-X. Chen, Y.-Y. Shen, and X.-M. Kong, *Phys. Rev. B* **82**, 174404 (2010).
- [54] X.-J. Yuan, X.-M. Kong, Z.-B. Xu, and Z.-Q. Liu, *Physica A* **389**, 242 (2010).
- [55] Y.-F. Li and X.-M. Kong, *Chin. Phys. B* **22**, 037502 (2013).
- [56] J. Florencio, S. Sen, and Z.-X. Cai, *J. Low. Temp. Phys.* **89**, 561 (1992).
- [57] J. Florencio and F. C. Sá Barreto, *Phys. Rev. B* **60**, 9555 (1999).
- [58] J. Florencio, O. F. A. Bonfim, and F. S. Barreto, *Physica A* **235**, 523 (1997).
- [59] Maria Eugênia Silva Nunes, É. M. Silva, P. H. L. Martins, J. A. Plascak, and J. Florencio, *Phys. Rev. E* **98**, 042124 (2018).
- [60] M. E. S. Nunes, E. M. Silva, P. H. L. Martins, J. Florencio, and J. A. Plascak, *Physica A* **541**, 123683 (2020).
- [61] M. H. Lee, J. Hong, and N. L. Sharma, *Phys. Rev. A* **29**, 1561 (1984).
- [62] N. L. Sharma and M. H. Lee, *J. Math. Phys.* **27**, 1618 (1986).
- [63] N. L. Sharma, *Phys. Rev. B* **45**, 3552 (1992).
- [64] M. H. Lee and J. Hong, *Phys. Rev. B* **32**, 7734 (1985).
- [65] M. H. Lee and J. Hong, *Phys. Rev. B* **30**, 6756 (1984).
- [66] M. H. Lee and J. Hong, *Phys. Rev. Lett.* **48**, 634 (1982).
- [67] J. Florencio and M. H. Lee, *Phys. Rev. A* **31**, 3231 (1985).
- [68] M. H. Lee, *Symmetry* **8**, 22 (2016).
- [69] M. B. Yu, *Phys. Lett. A* **380**, 3583 (2016).
- [70] M. B. Yu, *Eur. Phys. J. B* **90**, 87 (2017).
- [71] M. B. Yu, *Eur. Phys. J. B* **91**, 25 (2018).
- [72] A. Wierling, *Eur. Phys. J. B* **85**, 20 (2012).
- [73] A. Wierling and I. Sawada, *Phys. Rev. E* **82**, 051107 (2010).
- [74] E. M. Silva, *Phys. Rev. E* **92**, 042146 (2015).
- [75] E. M. Silva, *Acta Phys. Pol. B* **46**, 1135 (2015).
- [76] V. S. Viswanath and G. Müller, *The Recursion Method—Application to Many-Body Dynamics*, 1st ed. (Springer-Verlag, Berlin, 1994), Vol. 23.
- [77] V. S. Viswanath and G. Müller, *J. Appl. Phys.* **67**, 5486 (1990).
- [78] U. Brandt and K. Jacoby, *Z. Phys. B* **25**, 181 (1976).
- [79] H. W. Capel and J. H. H. Perk, *Physica A* **87**, 211 (1977).
- [80] R. Kubo and K. Tomita, *J. Phys. Soc. Jpn.* **9**, 888 (1954).
- [81] A. Bencini and D. Gatteschi, *EPR of Exchange Coupled Systems* (Dover, New York, 2012).
- [82] A. Zorko, Determination of Magnetic Anisotropy by EPR, in *Topics from EPR Research*, edited by A. M. Maghraby (IntechOpen, London, 2019), Chap. 3, pp. 23–43.